



OPEN

Gastric functional monitoring by gastric electrical impedance tomography (gEIT) suit with dual-step fuzzy clustering

K. Sakai¹, P. N. Darma^{2✉}, P. A. Sejati¹, R. Wicaksono¹, H. Hayashi³ & M. Takei¹

Gastric Function has been successfully estimated by gastric electrical impedance tomography (gEIT) Suit with dual-step fuzzy clustering. The gEIT Suit which are made of elastic cloth with dual-planar electrodes and compact data acquisition (DAQ) system measures gastric impedance Z to visualize the gastric conductivity distribution σ . The dual-step fuzzy clustering extracts the clustered gastric conductivity distribution $^k\sigma$, which accurately estimates the gastric function. The gEIT Suit with dual-step fuzzy clustering are applied to eight healthy persons during liquid meal consumption to estimate the gastric function under gastric accommodation phase of 200, 400 and 600 mL based on the gastric emptying phase. As the results, the gEIT Suit successfully estimate the gastric function. By the measured impedance Z , the subjects have a mean temporal impedance $\overline{\Delta Z} = -9.27$ [Ohm] and p -value of that $\overline{Z} p(Z) = 0.0013[-]$ as the t-test result. In the case of gastric conductivity distribution σ , the subjects have a value of spatial mean conductivity distribution $\langle \sigma \rangle = 0.23[-]$ and p -value of that $\langle \sigma \rangle p(\sigma) = 0.0140[-]$. Lastly, in the case gastric volume V , subjects have a gastric volume $V = 12.44$ [%] and p -value $p(V) = 0.0664[-]$.

Monitoring of gastric function by measuring¹ is a critical parameter in many clinical conditions such as aspiration of gastric content during anesthesia², gastroesophageal reflux diseases³, gastroparesis diseases⁴, and functional dyspepsia diseases⁵ to estimate gastric function. Proper daily monitoring of gastric function is necessary to improve the patient's quality of life. Several methods are currently used to monitor gastric function, which are Electro Gastro Graphy (EGG), intra-gastric barostat (IGB), dynamic magnetic resonance imaging (MRI). The EGG is the noninvasive technique of electro physiological used to record gastric function by electrical activity measured from electrodes placed on the surface of abdomen as a representation of the gastric function⁶. The Electrical Impedance Tomography is also the noninvasive and electrical technique to evaluate gastric function. The intra gastric barostat is considered as the golden standard to directly measure gastric function using polyethylene bag implanted in the proximal stomach through inflation or deflation of the polyethylene bag. During emptying phase, the intra gastric barostat detects decreasing of polyethylene bag volume as the results of increasing pressure in the proximal stomach⁷. MRI determines gastric function level using interaction of magnetic field and particle properties inside stomach, then simultaneous MRI scans the abdomen to determine gastric functional activity through MRI volumetric image reconstruction⁸. On the other hand, ultrasound determines gastric function level using reaction of emitted ultrasound, then ultrasound scans on the abdomen to determine the gastric function through combination of several number of 2D images through movement of ultrasound transducer array on the stomach⁹. Nonetheless, these current standard methods have some drawbacks which are invasive, radioactive, expensive and massive which are impractical for daily monitoring of gastric function.

In order to solve problem that there is no daily gastric function measurement method, because conventional techniques are not suitable: expensive, large, invasive, for monitoring gastric function, a recent development in electrical impedance tomography (EIT)¹⁰ and mobile data acquisition systems¹¹ has opened the possibility of daily gastric morphological imaging. EIT has been successfully applied as an alternative bio-medical morphological imaging such as functional lung imaging¹², muscle imaging¹³, and breast cancer imaging¹⁴, abdomen subcutaneous fat imaging¹⁵, and urinary bladder imaging¹⁶.

¹Department of Mechanical Engineering, Graduate School of Science and Engineering, Chiba University, Chiba-Shi, Japan. ²Division of Fundamental Engineering, Department of Mechanical Engineering, Graduate School of Science and Engineering, Chiba University JSPS International Research Fellow, Chiba-Shi 263-8522, Japan. ³Center for Frontier Medical Engineering, Chiba University, Chiba-Shi, Japan. ✉email: panji.nursetia@chiba-u.jp

Tissue	Conductivity [S/m]	Permittivity [-]
Fat	0.042	911.5
Kidney	0.137	38748.0
Liver	0.053	28
Skin	0.0002	1133.5
Spinal cord	0.004	35568.9
Spleen	0.110	13891.2
Gastric	0.530	8698.7

Table 1. Dielectric properties of human abdomen tissues ¹⁷.

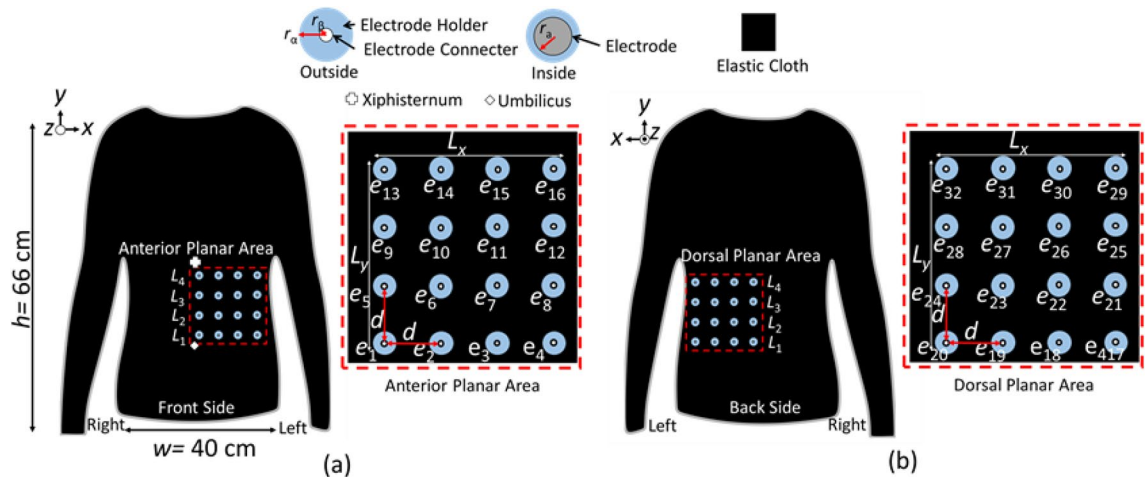


Figure 1. Concept of gEIT suit (a). Anterior planar area (b) Dorsal planar area.

Although EIT is able to image human body parts such as the lung, muscle, breast, subcutaneous abdominal fat and urinary bladder, it is extremely difficult to apply EIT to human gastric functional monitoring, since the human stomach is located near to multiple layers of organs which have similar electrical properties, such as the kidney, liver, skin, spinal cord and spleen, as shown in Table 1¹⁷, that conductivity are only 1/4 or more smaller than gastric conductivity. Those abdomen organs surrounded gastric make gastric conductivity distribution image by EIT noisy.

In order to resolve the difficulties, mitigate influence from gastric surrounded organs and clear noise from EIT image, we already proposed gastric electrical impedance tomography (gEIT) method by 3D full Jacobian matrix **J** and dual-step fuzzy clustering for extracting gastric function in-vitro experiments during gastric empty phases, fundus relaxation phase, corpus relaxation phase and antrum relaxation phase¹⁸.

However, our previous gEIT method has several drawbacks to apply to a real gastric human imaging such as (1) the static gEIT sensors were used in the experimental study using typical abdomen geometry with the electrodes were placed in the rigid position. On the other hand, the electrodes should be placed around an abdomen segment with a flexible shape and different sizes in gastric function monitoring. (2) the huge and heavy impedance analyzer was used to measure the impedance during the experimental study. On the other hand, measurement equipment should be smaller for easy using as daily gastric function monitoring.

In this paper, a non-invasive gEIT Suit is applied to estimate gastric function in eight healthy subjects during gastric emptying phase through overnight fasting and gastric accommodation phase. The proposed method has 2 stages which are (1) fabrication of gEIT Suit by integration of elastic suit with dual-planar EIT electrode arrangement with compact data acquisition (DAQ) system to measure the impedance **Z**, and (2) reconstruction of gastric conductivity distribution σ with dual step fuzzy clustering estimate the gastric volume *V*.

Gastric EIT (gEIT) suit with dual-step fuzzy clustering

Fabrication of gEIT suit. Figure 1 shows the concept of gEIT Suit to visualize gastric conductivity distribution inside abdomen. gEIT Suit has a function to measure impedance **Z** by using *E* (*E* = 32 as an example in the Fig. 1) number of electrodes *e_e* along the abdomen surface. The gEIT Suit consist of elastic cloth (black colour), electrodes holder (blue colour), electrodes connector (white colour) and electrodes (grey colour). The elastic cloth is composed of 88% polyester and 12% polyurethane material with initial width *w* = 40 [cm] and height *h* = 66 [cm], when the elastic cloth is stretched, the maximum width *w_{max}* = 56 and maximum height *h_{max}* = 88 cm. The electrodes *e₁, e₂, ..., e₃₂*, (*E* = 32 in the figure as an example) with radius *r_e* = 8 [mm] are attached across the elastic cloth on the abdomen surface to measure the Impedance **Z**. The electrodes are covered with electrode holder α with radius *r_α* = 1 [cm] made by Poly Lactic Acid (PLA) material to fix the electrode posi-

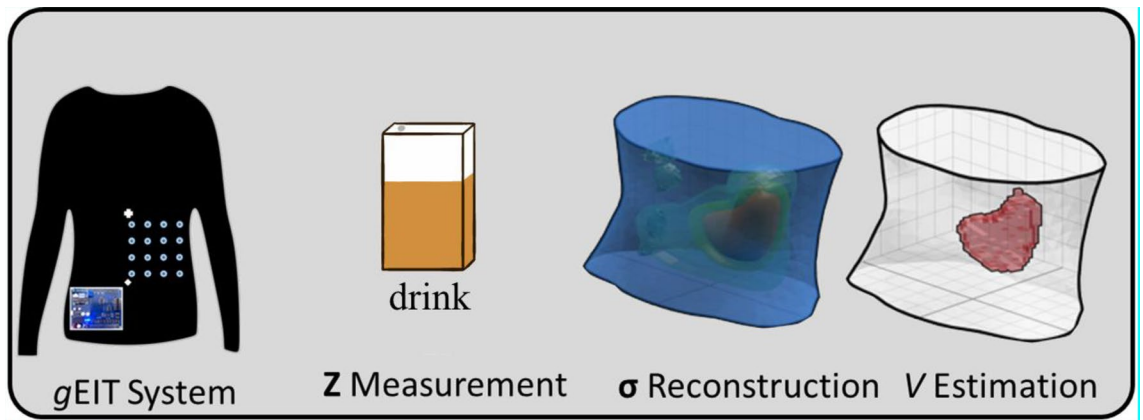


Figure 2. Overview of gastric content volume V estimation by gEIT Suit with dual-step fuzzy clustering.

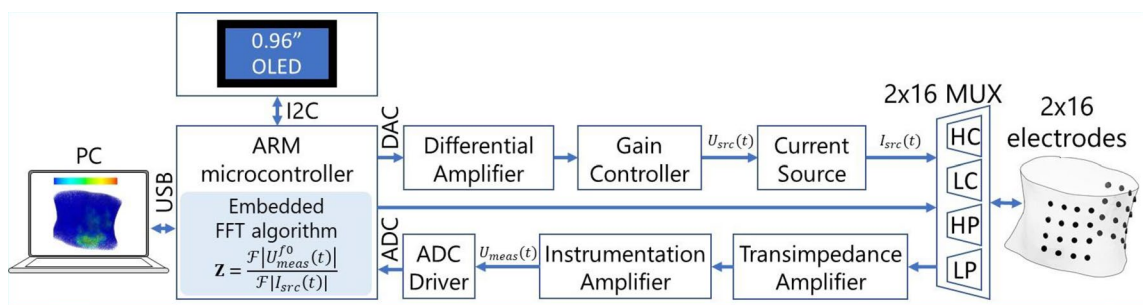


Figure 3. The block diagram of gEIT hardware.

tion on elastic cloth surface. Furthermore, the electrode connector β with radius $r_\alpha = 2$ [mm] is attached on the centre of electrode holder to connect the electrodes with compact gEIT DAQ cables.

The electrodes are arranged according to dual planar configuration as shown in Fig. 1 consist of anterior planar area Fig. 1a in the front side of gEIT Suit and dorsal planar area on back side of gEIT Suit Fig. 1b with horizontal area length $L_x = 17$ [cm] and vertical area length $L_y = 17$ [cm]. Each planar consists of 16 electrodes.

Compact data acquisition (DAQ) system. Figure 2 shows the compact gEIT DAQ system hardware which is connected to elastic suit through electrodes. Further, Fig. 3 shows the block diagram of gEIT hardware. The compact gEIT DAQ consists of advanced RISC (reduced instruction set computer) machine (ARM) microcontroller, differential amplifier, gain controller, current source, multiplexers (MUX), trans-impedance amplifier, instrumentation amplifier, and ADC driver. The main controller of compact gEIT DAQ is ARM Cortex-M4-based microcontroller with 180 MHz clock speed. The compact gEIT DAQ has capability to generate the digitized sinusoidal signal through a 10-bit analogue to digital converter (DAC) which then converted to analogue voltage source $U_{src}(t)$ by differential amplifier and gain controller. In order to perform the constant current injection, $U_{src}(t)$ is converted into current source $I_{src}(t)$ by general Howland current circuit. The $I_{src}(t)$ injection and voltage measurement $U_{meas}(t)$ operation is handled by 2×16 analogue multiplexers (MUX), which are divided into four section: high current (HC), low current (LC), high potential (HP), and low potential (LP). The ARM microcontroller controls the injection and measurement pattern¹⁵.

The compact gEIT DAQ measured voltage at t -th time $U_{meas}(t)$ is processed by trans-impedance and instrumentation amplifier converted into acceptable ARM microcontroller voltage level by analog to digital converter (ADC) driver. The real-time measurement of $U_{meas}(t)$ is measured by the 12-bit ADC of the controller. Then, the Z measurement is performed by conducting an embedded fast Fourier transform (FFT) algorithm which expressed as,

$$Z = \frac{\mathcal{F}|U_{meas}^{f0}(t)|}{\mathcal{F}|I_{src}(t)|} \tag{1}$$

where \mathcal{F} is the Fourier transform of given fundamental $U_{meas}(t)$ signal $U_{meas}^{f0}(t)$ at the time domain¹⁹. The measured Z then sent into PC through USB connection by universal asynchronous receiver-transmitter (UART) at 1,000,000 bps. The specification of gEIT hardware is summarized in Table 2¹⁹.

Estimation of gastric function by dual-step fuzzy clustering based on reconstructed images. In this stage, the conductivity distribution σ is clustered using the dual-step fuzzy clustering into

Parameter	Value
Measurement speed	10 fps
Frequency	100 Hz ~ 200 kHz
Current injection	1 mA (constant)
Digital signal processing (DSP)	Embedded FFT algorithm
UART baud rate	1,000,000 bps
I/O channel	2 × 16 channels
Switching mode	Full 3D Injection

Table 2. Specification of hardware.

three clusters ${}^k\sigma$ ($k=3$) which are gastric content ${}^1\sigma$, gastric wall ${}^2\sigma$, and other abdomen organs ${}^3\sigma$ ¹⁸. The objective of the first step of fuzzy clustering is to eliminate noise conductivity from abdomen organs can be summarized using the following equations:

$${}^k\mathbf{r}_c^j = \frac{\sum_{nk=1}^{nk=Nk} {}^k\sigma_n \mathbf{r}_n}{\sum_{nk=1}^{nk=Nk} {}^k\sigma_n} \quad (2)$$

$${}^k\mathbf{f}_c^j = \frac{\sum_{n=1}^{n_k} ({}^k\mu_n^j)^2 {}^k\sigma_n \mathbf{r}_n}{\sum_{n=1}^{n_k} ({}^k\mu_n^j)^2} \quad (3)$$

$${}^k\mu_n^j = 1 / \sum_{l=1}^{l=k} \left(\frac{\|\mathbf{r}_n - {}^k\mathbf{r}_c^j\|}{\|\mathbf{r}_n - {}^l\mathbf{r}_c^j\|} \right)^2 \quad (4)$$

$${}^k\sigma = \arg \min \sum_{k=1}^{k=K} \sum_{n=1}^N ({}^k\mu_n^j)^2 \|\mathbf{r}_n - {}^k\mathbf{f}_c^j\|^2 \quad (5)$$

$${}^k\mathbf{f}_c^{j+1} - {}^k\mathbf{f}_c^j = 0 \quad (6)$$

where ${}^k\mathbf{r}_c^j$ in (2) is k -th clustered centroid position at j -th iteration number, ${}^k\sigma_n$ is k -th clustered conductivity distribution at n -th elements, $\mathbf{r}_n = [x_n, y_n, z_n]$ is n -th mesh element position vector, n_k ($1 \leq n_k \leq N_k$) is the n -th mesh which belongs to ${}^k\sigma$. At fuzzy centroid calculation process, fuzzy centroid position of k -th cluster ${}^k\mathbf{f}_c^j$ from the n -th mesh element position vector ${}^k\mathbf{r}_n$ is calculated by (3) and (4). Then, the elements of ${}^k\sigma_n$ are relocated into a new clustered conductivity distribution by calculating Euclidean distance between the position of \mathbf{r}_n and ${}^k\mathbf{f}_c^j$ by (5). The final clustered conductivity distribution is achieved while the difference between ${}^k\mathbf{r}_n^j$ and ${}^k\mathbf{r}_n^{j+1}$ equal to 0 as shown in Eq. (6). Finally, the second dual-step fuzzy clustering is started by extracting the only gastric conductivity distribution ${}^*\sigma$ by eliminating the conductivity noise from abdomen organs ${}^3\sigma$ using following equation

$${}^*\sigma_n = \begin{cases} 0, & \sigma_n \in {}^3\sigma \\ \sigma_n, & \sigma_n \notin {}^3\sigma \end{cases} \quad (7)$$

Experiment setup and protocol

Experimental setup. Figure 4 shows the experimental setup consisting of a) gEIT Suit composed of elastic suit fabricated in the stage 2A, a compact gEIT DAQ developed in the stage 2B and a Personal Computer (Mouse Computer LM-iH800) with 3.2 GHz Intel Core i7-8700 and 64 Gb RAM was used in the reconstruction of gastric conductivity distribution by gEIT Suit and estimate the gastric volume V by Fuzzy Clustering.

Experimental protocol. Eight healthy young men (age: 25 ± 5 years, body mass index 21.94 ± 3.27) volunteered for this study. Figure 5 shows the experimental protocol consist of two phases: gastric empty phase and gastric accommodation phases using gEIT Suit measurement Fig. 4a and ultrasound measurement system Fig. 4b.

Gastric empty phase is defined as measurement of the gastric area during fasting condition (no meal or drink) for at least 8 h, on the other hand the gastric accommodation phases is defined as the measurement of gastric area using 200 mL, 400 mL and 600 mL liquid meal (Aisokaru 100, Nestle Health Science Japan) Measurement of ultrasound area of the antrum was obtained by abdominal ultrasound probe (frequency 4 MHz) manufactured by GE Healthcare.

In all experiment parts, volunteered subjects were measured in a standing position. Chiba University Ethic Research Committee approved this protocol and all volunteers gave informed written consent before experiments. All study procedures were conducted in accordance with the Declaration of Helsinki. The subjects were

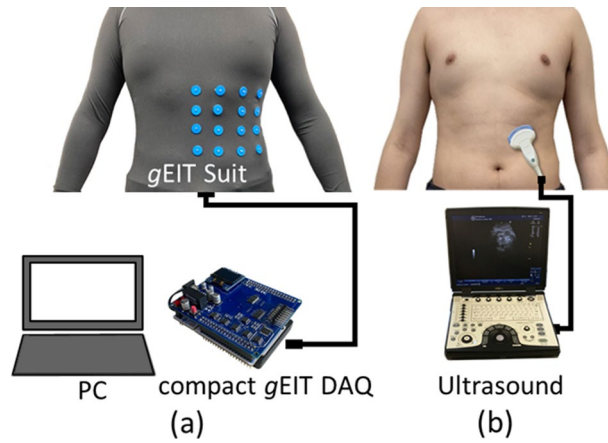


Figure 4. Experimental Setup (a) gEIT system experimental setup, (b) ultrasound experimental setup.

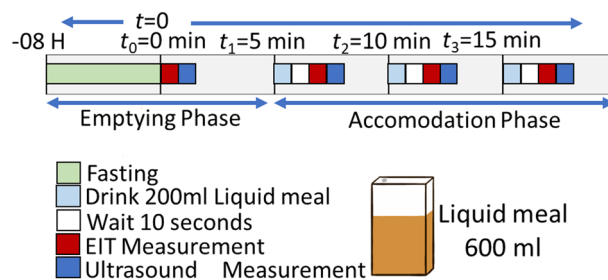


Figure 5. Experimental protocol.

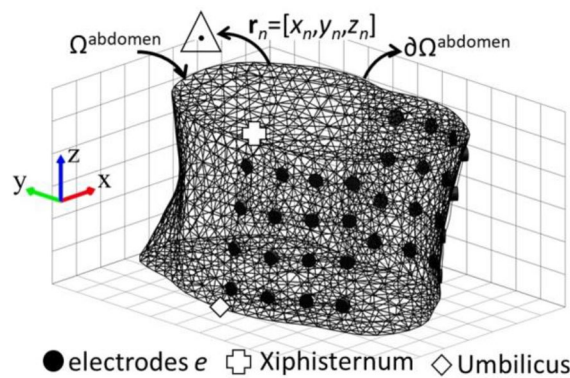


Figure 6. 3-dimensional mesh inside abdomen Ω_{abdomen} .

asked to fast for at least 8 Hours and avoid to drink alcohol, caffeine and any medication that could affect their gastric function in the gastric emptying phase. The subjects underwent the gastric emptying scan at 8 h + 0 min (t_0) followed by gEIT Suit measurement and ultrasound measurement. After that the gastric accommodation start at 8 h + 5 min (t_1) by drinking 200 mL of liquid drink followed by gEIT Suit and US measurements. Next in the 8 h + 10 min (t_2), the subject were asked to drink 200 mL of liquid meal followed by gEIT Suit and US measurements. Lastly, in the 8 h + 15 min (t_3), the subject were asked to drink 200 mL of liquid meal followed by gEIT Suit and US measurements.

Image reconstruction method. Figure 6 shows the structure of gEIT Suit around an abdomen boundary $\partial\Omega_{\text{abdomen}}$ with electrodes number e ($1 \leq e \leq E, E = 32 = 8 \text{ electrodes per one layer} \times 4 \text{ layers}$ as an example in Fig. 6. The abdomen inside is discretised into volumetric elements with number N as shown in Fig. 6. In order to obtain conductivity distribution by gEIT, time difference (td-gEIT) Gauss–Newton image reconstruction is used using following equation

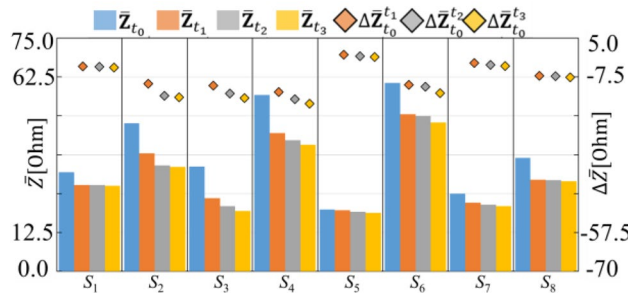


Figure 7. Comparison of average measured impedance \bar{Z} , delta measured impedance $\Delta\bar{Z}$.

$$\sigma^{j+1} = \sigma^j - \left(\mathbf{J}^T \mathbf{J} + \lambda \mathbf{R} \right)^{-1} \mathbf{J}^T \Delta \mathbf{Z} \tag{8}$$

where \mathbf{R} is a regularization matrix, and λ is a relaxation factor scalar which is automatically determined by L-Curve method²⁰, $\Delta \mathbf{Z} = [\Delta Z_1, \dots, \Delta Z_m, \dots, \Delta Z_M]^T \in \mathbb{R}^M$ is the normalized measured impedance between the impedance at initial time t_0 and measurement time t which is written by

$$\Delta Z_m(t - t_0) = \frac{Z_m(t) - Z_m(t_0)}{Z_m(t_0)} \tag{9}$$

where m is measured voltage pattern and M is total number of measurement patterns.

Experimental results and discussion

Gastric impedance. Based on the impedance measurement in chapter 2, Fig. 7 shows average measured impedance and delta measured impedance. The blue bar chart in the Fig. 7 indicates the average impedance during empty stomach at t_0 (\bar{Z}_{t_0}). On the other hand, the orange, grey and yellow bar chart represents the average impedance during the accommodation phase when the subjects were drinking 200 mL, 400 mL and 600 mL of a liquid meal at t_1 (\bar{Z}_{t_1}), t_2 (\bar{Z}_{t_2}), and t_3 (\bar{Z}_{t_3}) respectively. According to the Fig. 7, the measured impedance during the empty phase \bar{Z}_{t_0} has the highest value as compared with the average impedance during the accommodation phase ($\bar{Z}_{t_1}, \bar{Z}_{t_2}, \bar{Z}_{t_3}$). Furthermore, during the accommodation phase, the \bar{Z} were gradually decrease at t_1, t_2, t_3 ($\bar{Z}_{t_1} > \bar{Z}_{t_2} > \bar{Z}_{t_3}$). In order to quantitatively evaluate the gEIT Suit to estimate gastric content volume, the delta impedance between gastric empty phase and accommodation phases were calculated using following equation :

$$\Delta \bar{Z}_{t_0}^t = \left(\sum_{m=1}^{m=M} Z_m(t) - Z_m(t_0) \right) / M \tag{10}$$

where $Z_m(t_0), Z_m(t_1)$ are the impedance measurement at m -th measurement pattern during empty and accommodation phase respectively.

The orange, grey and yellow diamond chart in the Fig. 7 represents the delta average impedance during the accommodation phase when the subjects were drinking 200 mL, 400 mL and 600 mL of liquid meal at t_1 ($\Delta \bar{Z}_{t_0}^{t_1}$), t_2 ($\Delta \bar{Z}_{t_0}^{t_2}$), and t_3 ($\Delta \bar{Z}_{t_0}^{t_3}$) respectively. By the gEIT Suit measurement, the average value of delta impedance is $\Delta \bar{Z} = -9.27$ [Ohm].

Gastric conductivity distribution. Based on the reconstruction of gastric conductivity distribution σ by using gEIT Suit in the chapter 2. Figure 8a show the comparison of σ . Based on the Fig. 8a the σ are well visualized.

In order to quantitatively evaluate the performance of gEIT Suit to measure gastric content volume, the spatial mean conductivity (σ) were calculated using following equation:

$$\langle \sigma \rangle_t = \left(\sum_{n=1}^{n=N} \sigma_n^t \right) / N \tag{11}$$

σ_n^t is the conductivity distribution in n -th mesh voxel at t accommodation phases.

Figure 9 shows the spatial mean gastric conductivity distribution (σ). The orange, grey and yellow bar chart represents the (σ) during the accommodation phase when the subjects were drinking 200 mL, 400 mL and 600 mL of liquid meal at t_1 ($\langle \sigma \rangle_{t_1}$), t_2 ($\langle \sigma \rangle_{t_2}$), and t_3 ($\langle \sigma \rangle_{t_3}$), respectively. Based on the Fig. 9, the average value of (σ)=0.23 [S/m].

Gastric Accommodation Volume. Based on the clustered gastric conductivity distribution $^k \sigma$ by using dual step fuzzy clustering in the chapter 2, Fig. 8b shows comparison of clustered gastric conductivity distribution between healthy subjects. According to the Fig. 8b the gastric volume are qualitatively visualized during the

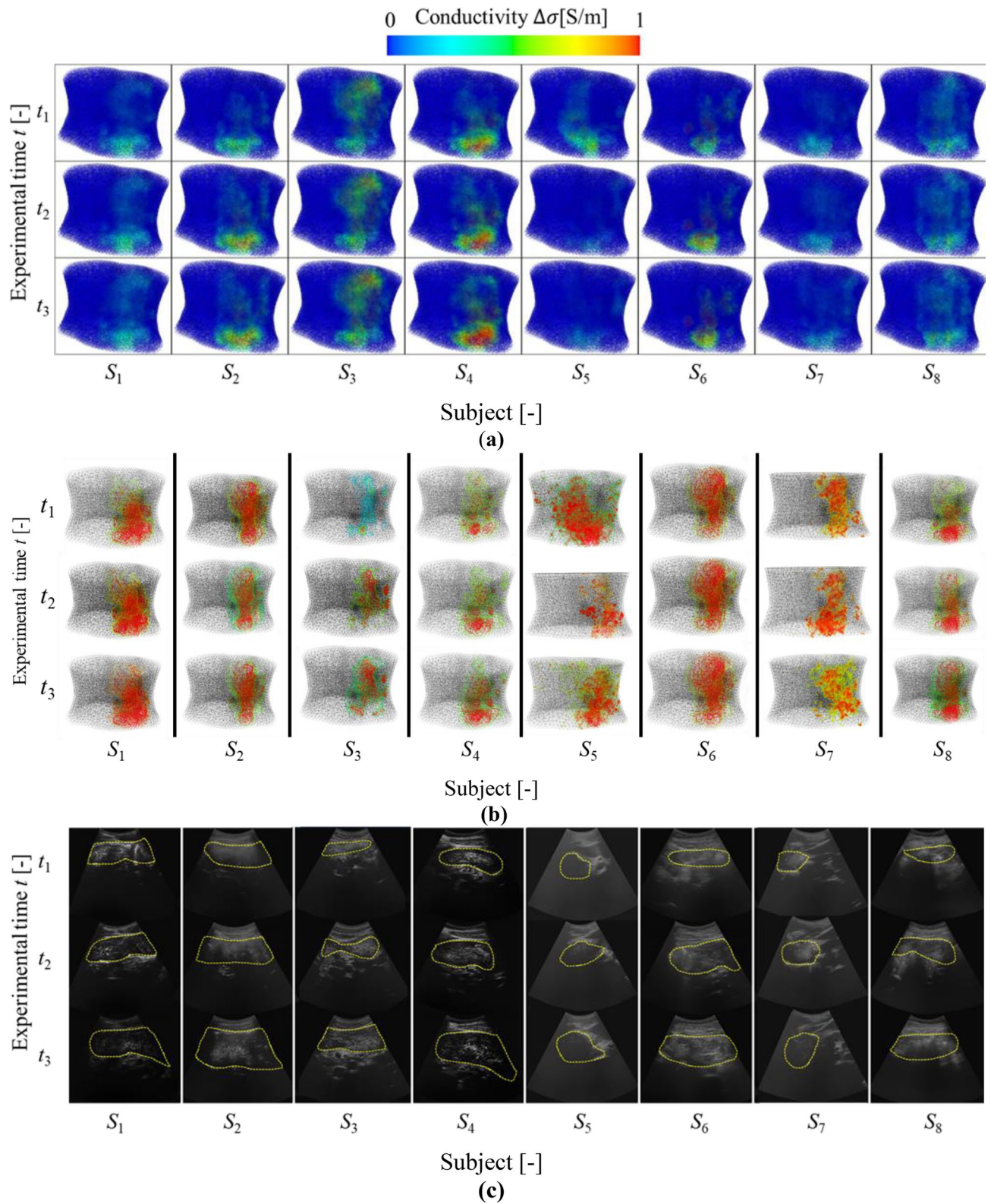


Figure 8. (a) Visualization of gastric conductivity distribution σ by gEIT Suit, (b) Extraction of clustered gastric conductivity distribution $^k\sigma$ by fuzzy clustering, (c) Evaluation of gastric area by ultrasound.

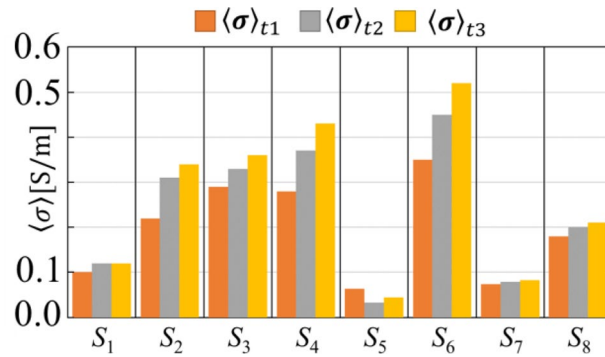


Figure 9. Spatial mean of gastric conductivity $\langle \sigma \rangle$ distribution.

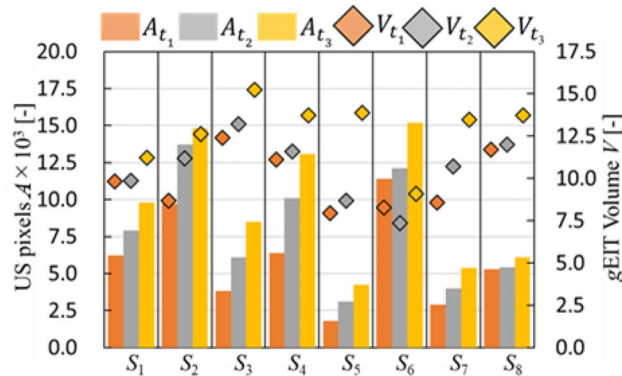


Figure 10. Comparison of gastric volume from gEIT suit V_t and gastric area from ultrasound A_t .

accommodation phases when the subjects were drinking 200 mL, 400 mL and 600 mL of liquid meal at t_1 (${}^k\sigma_{t_1}$), t_2 (${}^k\sigma_{t_2}$), and t_3 (${}^k\sigma_{t_3}$) respectively.

In order to quantitatively evaluate the performance of gEIT Suit to measure gastric content volume, the gastric volume V_t is defined using following equation:

$$V_t = \left(\frac{{}^k\sigma_t}{N} \right) \times 100\% \tag{12}$$

where ${}^k\sigma_t$ is the number of voxel in the clustered gastric conductivity at t -th time, N is total number of mesh inside the gEIT Suit boundary. Figure 10 shows the gastric volume from gEIT Suit between subjects and also gastric area from ultrasound measurement. Furthermore, Fig. 8c shows the comparison of gastric ultrasound images of healthy subjects. In order to quantitatively evaluate the gastric ultrasound images, the gastric area A_t is defined as the total pixels inside the gastric boundary (dashed yellow line) in the ultrasound images. The Pearson correlation r is defined using the following equation

$$r = \frac{1}{T} \sum_{t=1}^{t=T} \frac{[(V_t - \bar{V})(A_t - \bar{A})]}{\sqrt{[(V_t - \bar{V})^2 - (A_t - \bar{A})^2]}} \tag{13}$$

where V_t is gastric volume from gEIT Suit at experimental condition t -th time. \bar{V} is mean of gastric volume by gEIT Suit. A_t is defined as the pixels inside the gastric boundary in the ultrasound images at experimental condition t -th time. \bar{A} is mean of A_t and so on Where $T=3$ is total number of measurements during the gastric accommodation phases. Figure 11 shows the comparison of Pearson correlation r among healthy subjects. Based on the figure, gEIT suit has good agreement with ultrasound images with average $r=0.88[-]$.

In order to quantitative evaluation of gEIT Suit measurement, t -test was also applied that evaluates the probability distribution of a hypothesis as shown in following equations:

$$\tau(Z) = \frac{\Delta Z_{t-t_0} \sqrt{S}}{\sqrt{\frac{1}{S} \sum_{s=1}^S ((Z_t^s - Z_{t_0}^s) - (\Delta Z_{t-t_0}))^2}} \tag{14}$$

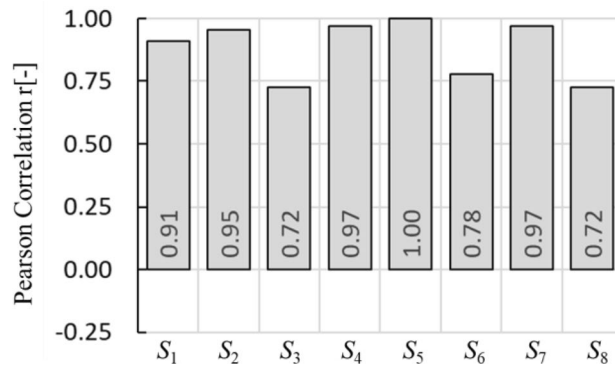


Figure 11. Comparison of Pearson correlation r .

Items	$\bar{Z}(t_3, t_0)$		$\langle \sigma \rangle(t_3, t_1)$		$V(t_3, t_1)$	
	t_3	t_0	t_1	t_3	t_1	t_3
Mean	29.7262	39.0041	11.8084	12.6070	0.1947	0.2634
SD	9.7906	13.6820	1.7405	1.9900	0.1013	0.1631
SE	3.4615	4.8373	0.6153	0.7036	0.0358	0.0577
Mean Diff	-9.2779		-0.7986		-0.0687	
$t_{0.025}$	2.1790					
t -value	-4.5927		-2.7643		-1.7939	
p -value	0.0013		0.0140		0.0664	

Table 3. Result of paired samples t -test for $\bar{Z}(t_3 - t_0)$, $\langle \sigma \rangle(t_3 - t_1)$, $V(t_3 - t_1)$.

$$\tau(\sigma) = \frac{\Delta\sigma_{t-t_0}\sqrt{S}}{\sqrt{\frac{1}{S} \sum_{s=1}^S ((\sigma_t^s - \sigma_{t_0}^s) - (\Delta\sigma_{t-t_0}))^2}} \tag{15}$$

$$\tau(V) = \frac{\Delta V_{t-t_0}\sqrt{S}}{\sqrt{\frac{1}{S} \sum_{s=1}^S ((V_t^s - V_{t_0}^s) - (\Delta V_{t-t_0}))^2}} \tag{16}$$

where τ is the t -test value of the mean impedance Z , spatial mean conductivity σ , gastric volume V , S is s subject number. Z_t^s is mean measured impedance by gEIT Suit at subject number s and t -th experimental condition, σ_t^s , V_t^s are same as spatial mean conductivity and gastric volume by gEIT Suit. ΔZ_{t-t_0} is mean of difference between experimental condition t , t_0 as $\Delta Z_{t-t_0} = \frac{1}{S} \sum_{s=1}^S (Z_t^s - Z_{t_0}^s)$. $\Delta\sigma_{t-t_0}$, ΔV_{t-t_0} are same at spatial mean conductivity and gastric volume. Finally, the probability value (p -value) $p(Z)$, $p(\sigma)$, $p(V)$, are obtained by $\tau(Z)$, $\tau(\sigma)$, $\tau(V)$.

Table 3 shows the result, the p -values obtained by t -test. $p(Z)$ and $p(\sigma)$ is extremely smaller than significance level 0.10 and $p(V)$ also smaller than that. So, null hypothesis are rejected. It can be say there is a significant difference between those mean value of Z , σ , V among experimental condition by gEIT Suit measurement.

Conclusions

Gastric functional monitoring has been proposed by Gastric Electrical Impedance Tomography (gEIT) Suit. The proposed method has 4 stages: (1) Fabrication of gEIT Suit by integration of elastic suit with dual-planar EIT electrode arrangement, (2) Measurement of gastric impedance Z by using compact gEIT data acquisition system (DAQ), (3) Reconstruction of gastric conductivity distribution σ by using time-difference gauss-newton algorithm and 4) Estimation of gastric volume V by using dual-step fuzzy clustering. The key finding of this research are :

1) By gEIT Suit measurement, the subjects have a value of temporal mean impedance $\Delta Z = -9.27$ [Ohm], spatial mean conductivity distribution $\langle \sigma \rangle = 0.23$ [-], and mean gastric volume $\bar{V} = 12.60$ [%].

2) The gEIT Suit statistically accurate with high pearson correlation mean value $r = 0.88$ [-] and low p -value $p(Z) = 0.0013$, $p(\sigma) = 0.0140$, $p(V) = 0.0664$ [-].

Data availability

The datasets used and/or analyzed during the current study available from the corresponding author on reasonable request. According to Bioethics Committee in Faculty of Engineering, Chiba University (ethical code R2-02), all subjects gave written informed consent for the study after receiving a detailed explanation for the purposes, potential benefits, and risks associated with participation. All study procedures were conducted in accordance with the Declaration of Helsinki and the research code of ethics of Chiba University and were approved by the Committee for Human Experimentation of Chiba University.

Received: 17 October 2022; Accepted: 23 December 2022

Published online: 10 January 2023

References

1. Buisman, W. J. *et al.* Evaluation of gastric volumes: Comparison of 3-D ultrasound and magnetic resonance imaging. *Ultrasound Med. Biol.* **42**(7), 1423–1430 (2016).
2. Bisinotto, F. M. B. *et al.* Use of ultrasound for gastric volume evaluation after ingestion of different volumes of isotonic solution. *Braz. J. Anesthesiol.* **67**(4), 376–382 (2017).
3. Clarrett, D. M. & Hachem, C. Gastroesophageal reflux disease affects millions of people worldwide with significant clinical implications. *Mo Med.* **115**(3), 214–218 (2018).
4. Soulsby, C. T. *et al.* Measurements of gastric emptying during continuous nasogastric infusion of liquid feed: Electric impedance tomography versus gamma scintigraphy. *Clin. Nutr.* **25**(4), 671–680 (2006).
5. Karamichou, E., Richardson, R. I., Nute, G. R., McLean, K. A. & Bishop, S. C. Genetic analyses of carcass composition, as assessed by X-ray computer tomography, and meat quality traits in scottish blackface sheep. *Anim. Sci.* **82**(2), 151–162 (2006).
6. Wolpert, N., Rebollo, I. & Tallon-Baudry, C. Electrogastrography for psychophysiological research: Practical considerations, analysis pipeline, and normative data in a large sample. *Psychophysiology* **57**(9), e13599 (2020).
7. Sarr M. G., Cullen J. J., Otterson M. F., Gastrointestinal motility. *Gastrointest. Anat. Physiol. Essent* 33–45, (2014).
8. Hoad, C. L. *et al.* Measurement of gastric meal and secretion volumes using magnetic resonance imaging. *Phys. Med. Biol.* **60**(3), 1367–1383 (2015).
9. Manini, M. L. *et al.* Feasibility and application of 3-dimensional ultrasound for measurement of gastric volumes in healthy adults and adolescents. *J. Pediatr. Gastroenterol. Nutr.* **48**(3), 287–293 (2009).
10. Darma, P. N., Baidillah, M. R., Sifuna, M. W. & Takei, M. Real-time dynamic imaging method for flexible boundary sensor in wearable electrical impedance tomography. *IEEE Sens. J.* **20**(16), 9469–9479 (2020).
11. Xu, Z. *et al.* Development of a portable electrical impedance tomography system for biomedical applications. *IEEE Sens. J.* **18**(19), 8117–8124 (2018).
12. de Gelidi, S. *et al.* Torso shape detection to improve lung monitoring. *Physiol Meas* **39**(7), 74001 (2018).
13. Sun, B. *et al.* Evaluation of the effectiveness of electrical muscle stimulation on human calf muscles via frequency difference electrical impedance tomography. *Physiol. Meas* **42**(3), 35008 (2021).
14. Hu, J. & Soleimani, M. Deformable boundary EIT for breast cancer imaging. *Biomed. Phys. Amp Eng. Exp.* **3**(1), 15004 (2017).
15. Lee, K., Yoo, M., Jargal, A. & Kwon, H. electrical impedance tomography-based abdominal subcutaneous fat estimation method using deep learning. *Comput. Math. Method Med.* **2020**, 1–14 (2020).
16. Sarker, S. A. *et al.* Noninvasive assessment of gastric acid secretion in man (application of electrical impedance tomography (EIT)). *Dig. Dis. Sci.* **42**(8), 1804–1809 (1997).
17. Gabriel, S., Lau, R. W. & Gabriel, C. The dielectric properties of biological tissues: II. Measurements in the frequency range 10 Hz to 20 GHz. *Phys. Med. Biol.* **41**(11), 2251–2269 (1996).
18. Darma, P. N., Kawashima, D., Takei, M. Gastric electrical impedance tomography (gEIT) based on a 3D jacobian matrix and dual-step fuzzy clustering post-processing. *IEEE Sens. J.*, 1–1, (2022).
19. Sejati, P. A. *et al.* On-line multi-frequency electrical resistance tomography (mfERT) device for crystalline phase imaging in high-temperature molten oxide. *Sensors* **22**, 1025 (2022).
20. Darma, P. N. & Takei, M. High-speed and accurate meat composition imaging by mechanically-flexible electrical impedance tomography with k-nearest neighbor and fuzzy k-means machine learning approaches. *IEEE Access* **9**, 38792–38801 (2021).

Acknowledgements

This work was supported by JSPS under postdoctoral fellowship of Japan Society for the promotion of science (JSPS) KAKENHI Grant Number 21F21356.

Author contributions

K.S. and P.N.D. wrote the main manuscript. P.A.S. and R.W. made hardware. H.H. and M.T. reviewed the manuscript.

Competing interests

The authors declare no competing interests.

Additional information

Correspondence and requests for materials should be addressed to P.N.D.

Reprints and permissions information is available at www.nature.com/reprints.

Publisher's note Springer Nature remains neutral with regard to jurisdictional claims in published maps and institutional affiliations.



Open Access This article is licensed under a Creative Commons Attribution 4.0 International License, which permits use, sharing, adaptation, distribution and reproduction in any medium or format, as long as you give appropriate credit to the original author(s) and the source, provide a link to the Creative Commons licence, and indicate if changes were made. The images or other third party material in this article are included in the article's Creative Commons licence, unless indicated otherwise in a credit line to the material. If material is not included in the article's Creative Commons licence and your intended use is not permitted by statutory regulation or exceeds the permitted use, you will need to obtain permission directly from the copyright holder. To view a copy of this licence, visit <http://creativecommons.org/licenses/by/4.0/>.

© The Author(s) 2022